Environmental Science and Pollution Research (2019) 26:4224–4233
https://doi.org/10.1007/s11356-018-1524-2

ADVANCED OXIDATION TECHNOLOGIES: STATE-OF-THE-ART IN IBERO-AMERICAN COUNTRIES

Toxicological study of the degradation products of antineoplastic agent etoposide in commercial formulation treated by heterogeneous photocatalysis using $SrSnO_3$

Idio Alves de Sousa Filho[1] · Tatiane Martins Lobo[1] · Cesar Koppe Grisolia[2] · Ingrid Távora Weber[1] · Marly Eiko Osugi[1,3]

Received: 23 October 2017 / Accepted: 9 February 2018 / Published online: 20 February 2018

Abstract

Etoposide is an antineoplastic agent used for treating lung cancer, testicular cancer, breast cancer, pediatric cancers, and lymphomas. It is a pollutant due to its mutagenic and carcinogenic potential. Disposal of waste from this drug is still insufficiently safe, and there is no appropriate waste treatment. Therefore, it is important to use advanced oxidative processes (AOPs) for the treatment and disposal of medicines like this. The use of strontium stannate ($SrSnO_3$) as a catalyst in heterogeneous photocatalysis reactions has emerged as an alternative for the removal of organic pollutants. In our study, $SrSnO_3$ was synthesized by the combustion method and characterized by X-ray diffraction (XRD), Raman, UV-Vis, and scanning electron microscopy (SEM) techniques, obtaining a surface area of 3.28 $m^2\ g^{-1}$ with cubic and well-organized crystallinity and a band gap of 4.06 eV. The experimental conditions optimized for degradation of an etoposide solution (0.4 mg L^{-1}) were pH 5 and catalyst concentration of 1 g L^{-1}. The results showed that the degradation processes using $SrSnO_3$ combined with H_2O_2 (0.338 mol L^{-1}) obtained total organic carbon removal from the etoposide solution, 97.98% ($\pm 4.03 \times 10^{-3}$), compared with TiO_2, which obtained a mineralization rate of 72.41% ($\pm 6.95 \times 10$–3). After photodegradation, the degraded solution showed no toxicity to zebrafish embryos through embryotoxicity test (OECD, 236), and no genotoxicity using comet assay and micronucleus test.

Keywords AOPs · Waste treatment · Antineoplastic · $SrSnO_3$ · Micronucleus test · Comet assay

Introduction

Drugs have marked a revolution in public health activities, reaching a prominent place in contemporary therapeutics (McEneff et al. 2014). Media incentive and the ease of acquisition made their use routine, generating an accumulation of these products in, households, while the residents are ignorant of the risks inherent to their storage and maintenance (Cabeza et al. 2012; Verlicchi et al. 2010) and unaware that improper disposal practices can cause environmental and public health damage. The casual discard of expired drugs, especially those with antineoplastic agents, may have as a consequence prominent environmental impacts, affecting several ecosystems (Hernando et al. 2006) and generating health risks, been cited as one of the major problems of modern society (McEneff et al. 2014; Ma et al. 2015; Oller et al. 2011; Cabeza et al. 2012).

Antineoplastic agents are used for the treatment of cancer, the second leading cause of death in Brazil, with an estimated 600,000 cases in 2018 (INCA 2018). The compounds present in these drugs are designed to be persistent; they must maintain their chemical characteristics throughout the time necessary to serve their therapeutic purpose (Lutterbeck et al. 2015; Araceli et al. 2010). This class of drugs deserves special

Responsible editor: Suresh Pillai

✉ Idio Alves de Sousa Filho
idiofilho@gmail.com

[1] Instituto de Química, Universidade de Brasília-UnB, Campus Darcy Ribeiro, Asa Norte, Brasília, DF CEP-70910-000, Brazil

[2] Instituto de Ciências Biologia, Departamento de Genética e Morfologia, Universidade de Brasília-UnB, Campus Darcy Ribeiro, Asa Norte, Brasília, DF CEP-70910-000, Brazil

[3] Unesp, Instituto Nacional de Tecnologias Alternativas para Detecção, Avaliação Toxicológica e Remoção de Micropoluentes e Radioativos (INCT-DATREM), Instituto de Química, Caixa Postal 355, Araraquara, SP 14800-900, Brazil

attention, since it has carcinogenic, genotoxic, and mutagenic effects even expired after their expiry date and even in very low concentrations (Lutterbeck et al. 2015; Araceli et al. 2010; Ocampo-Pérez et al. 2010; Yurdakal et al. 2007; Buerge et al. 2006). This makes them environmentally important compounds.

Due to the variety of neoplasms, a large number of antineoplastics are used for chemotherapy, including etoposide (Lutterbeck et al. 2015; Nussbaumer et al. 2011; Araceli et al. 2010). Etoposide is a semi-synthetic derivative of podophyllotoxin, a compound extracted from the roots and rhizomes of *Podophyllum peltatum* and *Paeonia emodi*. The structure and chemical formula $C_{29}H_{32}O_{13}$ are shown in Fig. 1. It is a cytotoxic drug whose mechanism of action is the inhibition of the topoisomerase II enzyme (Stahelin and Vin 1991). Etoposide is widely used in chemotherapy for a variety of tumors, including lung, testicular, gastric tract, ovarian, retinoblastoma, and leukemia (Stahelin and Vin 1991; Solano et al. 2012).

The control of disposal and storage for most expired drugs is still insufficient, and the lack of appropriate waste treatment is a complex challenge (Ocampo-Pérez et al. 2010; Araceli et al. 2010). Thus, there is a need to explore processes and the most effective techniques for wastewater treatment. Advanced oxidative processes are useful in removing pollutants as they have shown satisfactory results in the removal of some organic compounds with high toxicity that are harmful to the environment, such as antineoplastic agents (Lutterbeck et al. 2015; Cavalcante et al. 2013; Ocampo-Pérez et al. 2010; Araceli et al. 2010).

Although the use of TiO_2 as a catalyst in AOPs is well described and known in the literature, it is necessary to search for new materials with photocatalytic properties that can be used in the treatment and removal of organic pollutants. Perovskites, a class of mixed oxides which have optical, electrical, and magnetic properties, have been explored as an alternative material with interesting photoluminescent and photocatalytic properties, making them a promising photocatalyst for AOPs (Junploy et al. 2013; Wang et al. 2007; Sales et al. 2014; Peña and Fierro 2001; Lee et al. 2012).

$SrSnO_3$ is a distorted orthorhombic perovskite, due to distortion in the SnO_6 octahedrons. This distortion promotes specific properties, which enable its application as a thermal stable capacitor, humidity and gas sensor, and as photoluminescent and photocatalytic material (Sales et al. 2014; Junploy et al. 2013; Lee et al. 2012; Zhang et al. 2006).

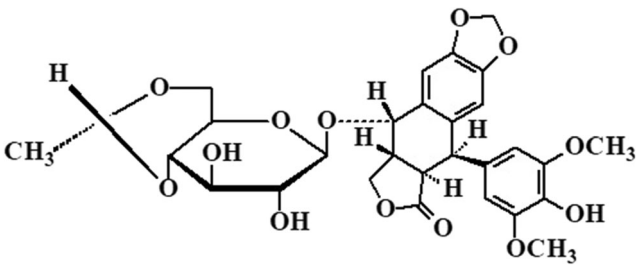

Fig. 1 Etoposide chemical structure

Although its use has grown, $SrSnO_3$ has not been investigated as a catalyst for degradation reactions of antineoplastic agents. Therefore, it is important to study and develop a methodology for applying $SrSnO_3$ as a catalyst, aiming for the degradation and total mineralization of these drugs, due to their high toxicity. Their complete elimination is necessary to reduce the problems arising from pollution and exposure, even in low concentrations. In the present study, the degradation of etoposide was investigated using the following AOPs: UV irradiation combined with H_2O_2 (UV/H_2O_2), heterogeneous photocatalysis ($UV/H_2O_2/SrSnO_3$), and direct photolysis. The assessment of toxicity is very important in AOPs, since degradation products can be generated, in some cases with higher toxicity than the initial product. The present study of toxicity was carried out using the fish embryo toxicity test (FET), comet assay, and micronucleus.

Materials and methods

Synthesis of $SrSnO_3$

$SrSnO_3$ was prepared by the combustion reaction, following the methodology described by Lobo et al. (2015). Strontium nitrate ($Sr(NO_3)_2$, Synth 99.9% purity) and tin chloride pentahydrate ($SnCl_4{\cdot}5H_2O$ Vetec 99.9% purity) were dissolved separately in distilled water and a solution of (2 mol L^{-1}), respectively. Both solutions were mixed, heated to 100 °C, and kept under constant magnetic stirring. Urea (Sigma-Aldrich, 98% purity) was then added. The molar stoichiometric ratios for Sr/Sn and Sr/urea were 1:1 and 1:4, respectively. The final solution was subjected to heating in a preheated oven (500 °C) for 60 min to promote a combustion reaction. The precursor powder was disaggregated and calcined at 800 °C for 150 min, using 10 °C min^{-1} as the heating rate and inertial cooling. After calcination, the samples were washed with an acetic acid solution (0.5 mol L^{-1}) and then with distilled water several times. The final product was filtered and dried at 70 °C for 360 min.

Characterization

Powder was characterized with an XRD (Bruker D8 Focus diffractometer operating with Cu K_α, $\lambda = 1.540619$ Å) and Raman spectroscopy (Renishaw spectrophotometer, inVia Raman Microscope—with Ar laser source, operating at 20 mW and 514.5 nm, one scan, exposure time 10,000 s), SEM (JEOL, model JSM 7001-F), UV-Vis diffuse reflectance spectroscopy (Varian Cary 5000 UV-Vis NIR, using $BaSO_4$ as reference—using the Tauc method (Tauc 1966) and specific

surface estimation by BET isotherms (Micromeritics Flowsorb II 2300hod.).

Photodegradation procedures

Photodegradation processes were conducted under seven different conditions: H_2O_2, $H_2O_2/SrSnO_3$ (absence light), UV, UV/H_2O_2, $UV/SrSnO_3$, $UV/SrSnO_3/H_2O_2$, and $UV/TiO_2/H_2O_2$. All tests were performed using 200 mL of aqueous solution of etoposide in commercial formulation in a concentration of 0.4 mg L^{-1}, in a photochemical reactor (Fig. 2) coupled to a recirculated thermostatic bath to keep the solution temperature constant at 25 °C. When necessary, UV radiation was provided by a 125-W (λ 254 nm) mercury vapor lamp without the bulb, with a photon incidence rate of 6.934×10^{19} photons s^{-1}, inserted into a quartz tube and immersed in the solution. The degradation was carried out in the following steps: (i) transfer of the solution to the reactor, (ii) addition of the catalyst ($SrSnO_3$), and, when necessary, (iii) addition 10 mL H_2O_2 (0.338 mol L^{-1}) at a flow rate of 0.0416 mL min^{-1} with the aid of a peristaltic pump (Cole Parmer, MasterFlex L/S model). The aliquots were collected hourly during the degradation experiment period and filtered through a nylon syringe microfilter (0.45-μm pore size, 13-mm diameter, Allcrom). These aliquots were analyzed with a Shimadzu TOC-L CPH/CPN (limit of detection 1 μg L^{-1}). Residual peroxide was determined using ammonium metavanadate (Nogueira et al. 2005), and residual absorbance H_2O_2 was measured in a UV-Vis at 452 nm. The catalyst reuse was evaluated by cycling the experiments up to three times. The catalyst was washed with distilled water several times, vacuum filtrated, and then thermally treated at 600 °C to remove residual organic material.

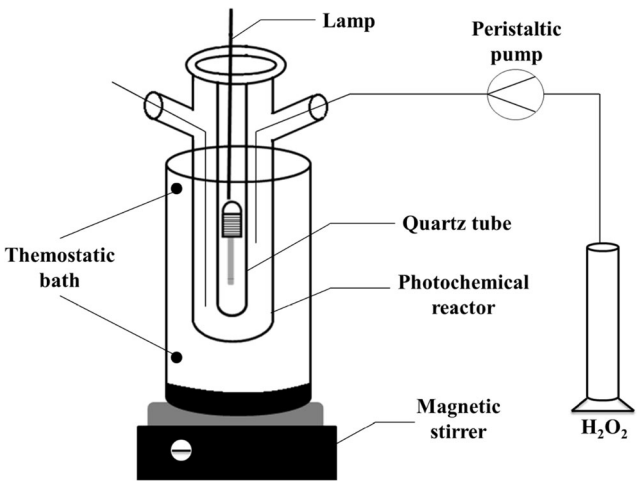

Fig. 2 Scheme of the photochemical reactor

Evolution of toxicity

Toxicity studies were performed using zebrafish embryos and adults from the facility of the Toxicological Genetics Laboratory (G-Tox) in the Institute of Biological Sciences at the University of Brasília. Adult zebrafish (*Danio rerio*) (6 months old) were maintained in a ZebTec housing system (Tecniplast Buguggiate, Varese, Italy) under controlled temperature (27 °C), pH (7.5), conductivity (740 μS/cm^2), and light/dark cycle (12:12 h). A fish embryotoxicity test (FET) was carried out according to OECD protocol no. 236 (OECD 2013). An initial solution (0.4 mg L^{-1}) and treated solution (residual), with seven dilutions (75, 50, 25, 10.1, 0.1, and 0.01%) were used in both studies. Exposures of adults were conducted in duplicate with six animals per tank of 6 L for 96 h in a static system. A nontreated control group was also included. All experiments used water from the ZebTec housing system. All physicochemical parameters (including the light/dark cycle) were monitored daily and kept constant during the exposures. At the end of the experiments, no mortality was observed and all fish were euthanized by immersion in an ice water bath. Peripheral blood samples were drawn with a heparinized syringe for comet assay and micronucleus test. For the embryotoxicity test, eggs were distributed into 24-well microplates: 20 wells were filled up with 2 mL of the test solution and 4 wells with water (internal plate control, as required in the OECD guideline). This test was initiated immediately after fertilization and was continued for 168 h. Embryos and larvae were observed daily under a stereomicroscope. Developmental parameters were evaluated on embryos over the test period using a magnification of × 70 for eggs and × 40 for hatched embryos. Before hatching, the following parameters were evaluated: egg coagulation, otolith formation, general delay in development, eye and body pigmentation, somite formation, heartbeat, edemas, detachment of the tail-bud from the yolk sac, yolk sac absorption, and hatching. After hatching, spine malformation and posture were also evaluated. All parameters were assessed and quantified as observed or not observed. Both studies had been previously approved by the institutional Animal Care and Use Committee (Institute of Biological Sciences, University of Brasilia), protocol number 82675/2011.

Adult fish were exposed to an etoposide commercial solution (0.4 mg L^{-1}) for the following bioassays: Comet assay carried out according to Kosmehl et al. (2008); in the test analysis, 100 cells per fish were counted and then analyzed with a fluorescence microscope (ZEISS Axioskop 2 - HAL 100), were counted, stained with ethidium bromide (20 μg mL^{-1}), and then analyzed. The cells were then classified according to the type of damage undergone (0, 1, 2, 3, and 4), using Comet IV software to calculate tail length. Micronucleus test, carried out according to Fenech et al. (2003), from peripheral blood samples were smeared on clean glass slides, dried at room

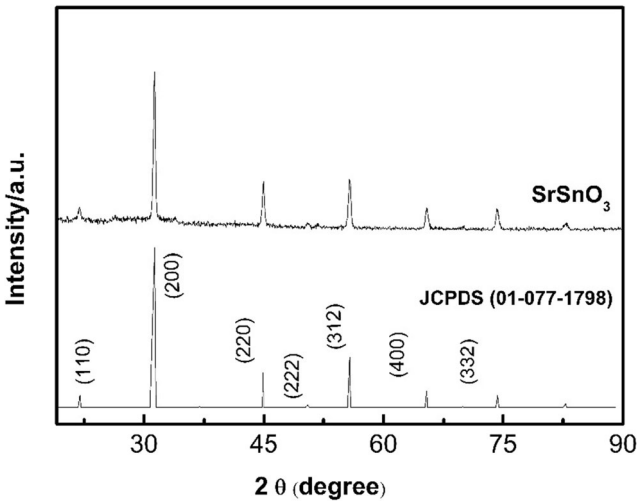

Fig. 3 Standard datasheet and diffraction pattern of synthesized $SrSnO_3$

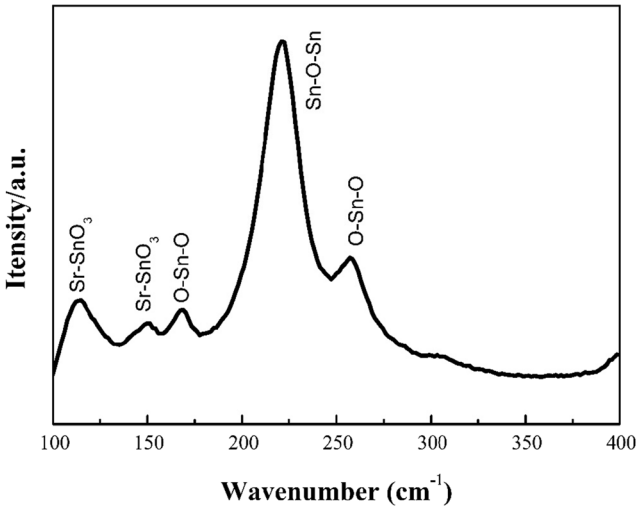

Fig. 4 Raman spectrum of as-prepared $SrSnO_3$ sample

temperature, fixed in ethanol for 7 min, and stained by Giemsa (5%). The slides were evaluated under a blind code; 3000 erythrocytes were microscopically scored for each sample at × 1000 of magnification (1500 erythrocytes per slide). The criteria for the identification of micronucleated erythrocytes of fish were as follows: area smaller than one third of the main nucleus; no connection with the main nucleus; no refraction and same color and color intensity as in the main nucleus. Erythrocytes were also scored to classify nuclear abnormalities (NAs). Among the most common NAs were bilobed nucleus (BN) and nuclear bud (NB).

Results and discussion

Photocatalyst characterization

The diffraction pattern was indexed as an orthorhombic perovskite (Fig. 3) (JCPDS 01-077-1798) in agreement with the (unbalanced) chemical reaction:

$$\mathrm{Sr(NO_3)_2 + SnCl_4 \cdot 5H_2O + CO(NH_2)_2(aq) \rightarrow SrSnO_3(s) + NO_x(g) + NH_3(g) + H_2O(g) + CO_2(g) + CO(g) + Cl_2(g)} \quad (1)$$

$^{*}\mathrm{NO_x = NO, NO_2}$

The powder presented high crystallinity, which benefits photocatalytic activity since it facilitates the migration of charged particles and disfavors the electron-hole recombination((h_{BV}^{+})/(e_{BC}^{-})) (Zhang et al. 2006; Lee et al. 2012).

The Raman spectrum of $SrSnO_3$ is shown in Fig. 4. Five bands related to the typical vibrational modes of perovskite were observed (Lucena et al. 2013; Alves et al. 2013): at 115, 146, and 170 cm^{-1} correspond to the Sr-SnO_3 network mode; at 222 cm^{-1} related to Ag mode which corresponds to the scissors movement of the Sn-O-Sn group along the c axis, and at 258 cm^{-1} related to the angular vibration of the O-Sn-O group at the *ab* plan and to the scissors movement at Sn-O-Sn perpendicular to the c axis. Additional lower intensity bands are observed at 304, 398, and 401 cm^{-1} and correspond to the torsion mode of SnO_3^{-2}.

A band gap value of 4.06 eV was obtained from Tauc (1966) plot, which agrees with previous reports in the literature (Lee et al. 2012; Sales et al. 2014). It nearly corresponds to the electronic transition from 2p oxygen orbital to 5 s tin orbital (Fig. 5) (Chen and Ye 2007).

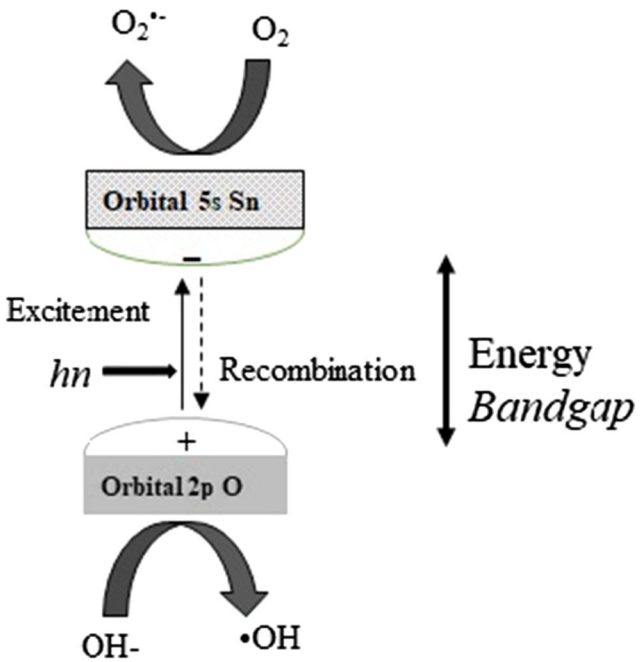

Fig. 5 Schematic representation of the electronic transition that occurs in $SrSnO_3$

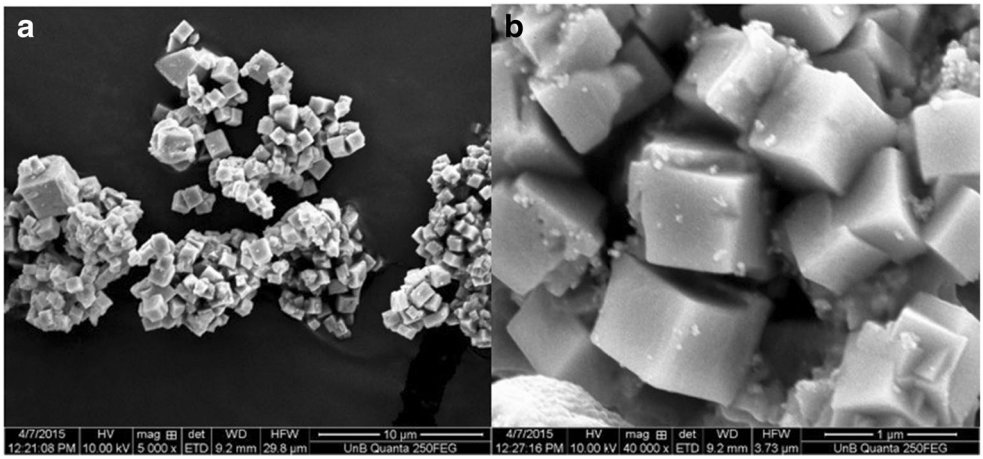

Fig. 6 Scanning electron micrograph of $SrSnO_3$ powder; **a** 5000× zoom, **b** 40,000× zoom

The band gap calculation was performed using Eqs. (2) and (3):

$$(\alpha.h.\nu)^{1/m} = A\left(h.\nu - E_g\right) \quad (2)$$

$$\alpha \propto F(\%R) = \frac{(1-\%R)^2}{2\cdot\%R} \quad (3)$$

where α is the absorption coefficient of the material; h is Planck's constant (6.626×10^{-34} J s); ν is the frequency of the incident radiation used in the analysis; A is a constant of proportionality; E_g is the energy of the optical band gap; and m is an integer depending on the type of electronic transition of most semiconductors, the value of the m used is ½ due to the fact that the studied electronic transition is direct and allowed.

In order to estimate α value for the studied UV-Vis interval, the Kubelka-MunK F (% R) function was used, which converts the percentage of reflectance (% R) into a measure directly proportional to α according to Eq. (3).

The sample presents a single phase, which has regular shapes and a good three-dimensional organization, referring to the crystallinity, as can be observed in Fig. 6a, b, being in agreement with the expected morphology for the material (Sales et al. 2014; Lobo et al. 2015). The particles were formed in a cubic structure. The surface area (S_{BET}) was estimated by N_2 adsorption isotherm (S_{BET}) was 3.28 $m^2\ g^{-1}$ in agreement with reports in the literature (Lobo et al. 2015; Sales et al. 2014; Hadjarab et al. 2007; Hodjati et al. 2000).

Etoposide degradation

First, a series of experiments varying the catalyst concentration were carried out. Five concentrations of catalyst were evaluated: 0.5, 0.75, 1, 5, and 10 g L^{-1}. The photodegradation tests were followed by an analysis of total organic carbon (TOC), as presented in Table 1. The concentration of 1 g L^{-1} had the best result, with a higher

Table 1 Study of the etoposide degradation solution 0.4 mgL^{-1} in different processes and degradation rate constants, $-k$ (h^{-1})

Process	Catalyst (g L^{-1})	pH	Mineralization %	k (h^{-1})	R
$UV/SrSnO_3$	0.5	5	$17.55 \pm 7.57 \times 10^{-3}$	0.0215	0.973
$UV/SrSnO_3$	0.75	5	$18.51 \pm 8.60 \times 10^{-3}$	0.0220	0.976
$UV/SrSnO_3$	1	5	$22.39 \pm 4.03 \times 10^{-3}$	0.0223	0.988
$UV/SrSnO_3$	5	5	$19.04 \pm 1.32 \times 10^{-2}$	0.0212	0.988
$UV/SrSnO_3$	10	5	$13.30 \pm 7.07 \times 10^{-5}$	0.0138	0.994
$UV/SrSnO_3$	1	3	$18.60 \pm 1.05 \times 10^{-2}$	0.0208	0.992
$UV/SrSnO_3$	1	12	$37.84 \pm 1.59 \times 10^{-2}$	0.0446	0.994
$UV/SrSnO_3/H_2O_2$	1	5	$97.98 \pm 4.03 \times 10^{-3}$	0.3795	0.998
$UV/SrSnO_3/H_2O_2$	1	12	$93.49 \pm 7.07 \times 10^{-3}$	0.0116[a]	0.997
$UV/TiO_2/H_2O_2$	1	5	$72.41 \pm 6.95 \times 10^{-3}$	0.1272	0.990
H_2O_2	–	5	$6.37 \pm 6.07 \times 10^{-3}$	0.004	0.994
$H_2O_2/SrSnO_3$	–	5	$8.27 \pm 4.87 \times 10^{-3}$	0.0092	0.994
UV	–	5	$4.36 \pm 7.64 \times 10^{-3}$	0.004	0.993
UV/H_2O_2	–	5	$55.49 \pm 1.93 \times 10^{-2}$	0.1278	0.849

[a] Second-order kinetics ($mg^{-1}\ h^{-1}$)

rate of mineralization. The results show that an increase in catalyst concentration decreases the rate of degradation due to the increased turbidity of the solution, damaging the passage of the radiation throughout the body of the solution and making it difficult to form h_{BV}^{+}/e_{BC}^{-} pairs (Konstantinou and Albanis 2004). A smaller amount of the catalyst facilitates the passage of the radiation throughout the body of the solution, activating a larger fraction of the catalyst and thus increasing its catalytic activity. The use of smaller amounts (0.5 and 0.75 g L^{-1}), however, results in a degradation lower than 1 g L^{-1} due to the contact area and the smaller amount of catalyst available for hydroxyl radical generation (Konstantinou and Albanis 2004).

For determination of the kinetics and degradation rate constant of the etoposide commercial solution, for pseudo-first-order reactions, the data were analyzed according to the graph of ln [TOC/TOC_0] vs time of treatment. For second-order reaction, the data were analyzed according to equation 1/[TOC] vs time. The interpretation of these results (Table 1) indicates that the degradations for most cases followed pseudo-first-order kinetics.

A second series of experiment was carried out, varying the pH. Approximately 1 g L^{-1} of $SrSnO_3$ for each pH at three pH values 3, 5, and 12, adjusting each according to the solution that would be degraded after addition of $SrSnO_3$. For pH 3 and 5, a solution of H_2SO_4 (8 mol L^{-1}) was used, and at pH 12, NaOH (8 mol L^{-1}) was used; the pH was adjusted only at the beginning before irradiation of UV light. Data in Table 1 indicate that the rate of degradation followed the following order: pH 12 > pH 5 > pH 3. This occurred due to the greater number of free hydroxyl ions that favored the formation of hydroxyl radicals and consequently the mineralization (Boczkaj and Fernandes 2017; Liu et al. 2017).

Favorable effects are expected with addition of H_2O_2 in photocatalytic processes; such effects are due to the reduction of hydrogen peroxide directly by the electrons of the conduction band or indirectly via superoxide ion radical, generating a radical HO•, as can be observed in Eqs. (4) and (5) (Zeng et al. 2016).

$$H_2O_2 + e_{BC} \rightarrow HO\bullet + OH^- \quad (4)$$

$$H_2O_2 + O_2^{\bullet -} \rightarrow HO\bullet + OH^- + O_2 \quad (5)$$

For solutions with pH > 5, by addition of hydrogen peroxide and UV radiation, there is an increase in the probability of hydroxyl radical generation, but pH < 3.5 favors hydrogen peroxide degradation, with consequent reduction in the efficiency of the process for these systems (Wu et al. 2004), thus justifying the nonuse of pH 3 combined with H_2O_2.

The interpretation of the results indicates that the degradation follows pseudo-first-order kinetics. The kinetic constants are presented in Table 1. The results indicated that the reaction rate using $SrSnO_3$ is higher than TiO_2. The UV/$SrSnO_3$/H_2O_2 process using pH 12 showed a pseudo-second-order kinetics, which indicates the existence of another variable besides the etoposide concentration, directly influencing the photocatalytic reaction process. This variable may be related to the increase in the presence of degradation products, a higher number of hydroxyl radicals, or even the amount of radical that has been generated.

The processes using H_2O_2 in the absence of UV radiation, photolysis, and UV/H_2O_2 were studied to evaluate the contribution of each to the photodegradation process (Table 1). The UV/H_2O_2 process is more efficient due to the breakdown of H_2O_2 molecules by UV radiation, which generates a greater amount of HO• radicals (Vogna et al. 2004).

Figure 7 shows the mineralization results of the degradation experiments conducted for each of the processes studied with the same parameters (radiation time, pH 5, 1 g L^{-1} catalyst, 0.338 mol L^{-1} H_2O_2).

The results show that the addition of H_2O_2 in the presence of $SrSnO_3$ with absence of light did not improve degradation. The process combined with UV light leads to almost complete degradation of the commercial etoposide solution. At the end of the process, the pH 5 presented a higher mineralization rate when compared to pH 12 (Table 1). This small difference between the mineralization rate for pH 12 when compared to pH 5 is probably derived from the dissociation of hydrogen peroxide (HO_2•) in the alkaline medium, reacting with hydroxyl radicals forming faster than hydrogen peroxide, thus making the process more efficient with higher pH, in solutions (Crittenden et al. 1999). As can be observed in Fig. 7, better results were found using $SrSnO_3$ than with TiO_2. There was a higher mineralization rate, and this result can be associated to the distortions presented in the structure of $SrSnO_3$, which can facilitate the transport of the carriers of loads, favoring the

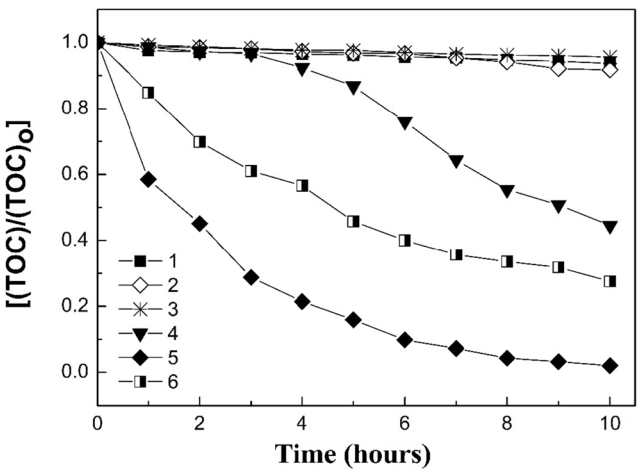

Fig. 7 Degradation of the etoposide solution (0.4 mgL^{-1}) by different AOPs, where 1, H_2O_2; 2, $SrSnO_3$/H_2O_2 (absence of light); 3, UV; 4, UV/H_2O_2; 5, $SrSnO_3$/H_2O_2/UV; 6, TiO_2/H_2O_2/UV

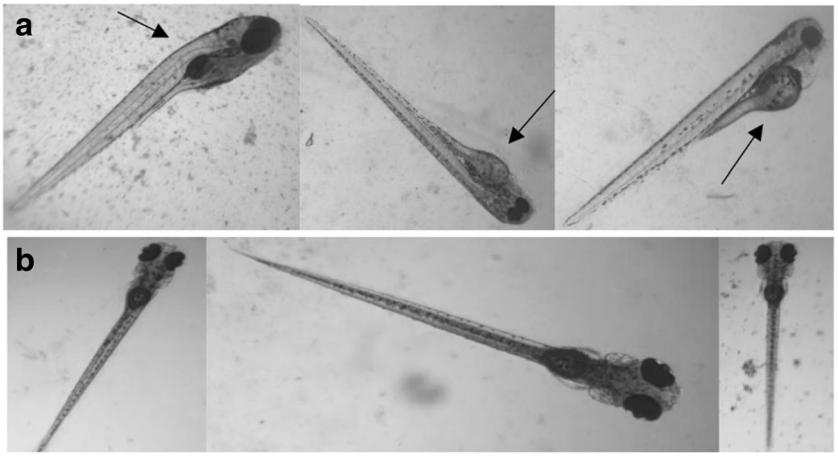

Fig. 8 **a** Embryos after 7 days of exposure to etoposide solution (0.4 mg L^{-1}). **b** Embryos after exposure to the solution after photocatalytic treatment

formation of hydroxyl radicals, which may confer advantages on their photocatalytic profile (Sales et al. 2014; Yuan, et al. 2007; Peña and Fierro 2001).

Adsorption tests showed that the drug adsorbed very little on the surface of $SrSnO_3$, with a reduction of 0.62% of TOC at the end of 6 h of exposure. So, an indirect mechanism should be seen as mainly responsible for the degradation of the commercial etoposide solution (Sales et al. 2014; Junploy et al. 2013). This indirect mechanism favored the generation of •OH, O_2•, and HO_2• radicals, formed from the water and oxygen adsorbed on the surface of the photocatalyst.

Studies of $SrSnO_3$ reuse were performed three times consecutively, with a decrease in catalytic activity of 7.55% at the end of the three processes. At the end of the degradation process, the resulting solution of the etoposide was added to the solution of the metavanadate ion. There was no color change at the end of the 10-h photodegradation, indicating that all the H_2O_2 initially added was completely consumed during the process.

Some studies have reported the use of $SrSnO_3$ for photocatalytic separation of water (Zhang et al. 2006; Lee et al. 2012) and discoloration of dyes (Sales et al. 2014; Lobo et al. 2015). To the best of our knowledge, however, this study represents for the first time that $SrSnO_3$ has been used to degrade antineoplastic agents.

Ecotoxicological tests of etoposide solution and its degradation products

The FET did not show embryotoxicity for the etoposide solution in commercial form since it did not present a mortality rate. Therefore, it was not possible to calculate the LC_{50}. Figure 8 shows the results obtained for the two solutions with 75% dilutions; in the others, there were no changes, after exposure of the embryos for 7 days. Although there was no mortality in the solution of the etoposide without treatment, there was a change in fish development, and the frequency of these changes was statistically different from the nonexposed organisms—ANOVA ($P \leq 0.001$).

Figure 8a shows that after 7 days of exposure to the etoposide solution, there was a significant interference in the development of the embryos when compared to Fig. 8b. The embryos exposed to the drug showed the poor formation of

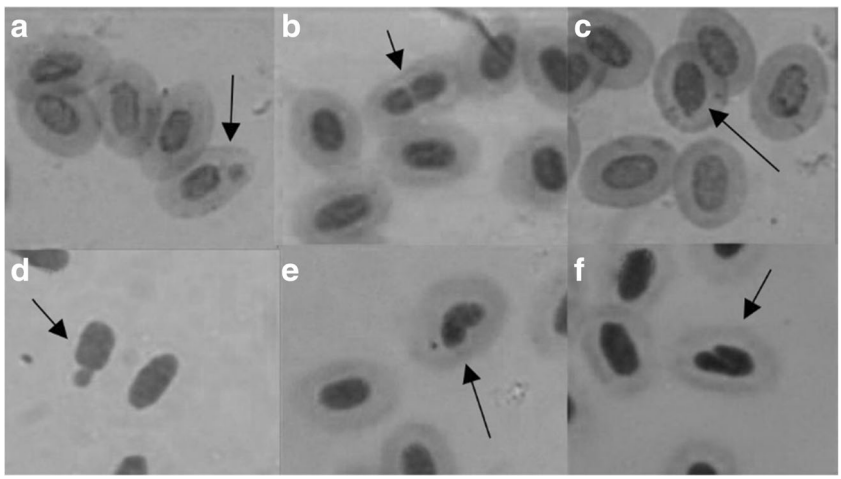

Fig. 9 Photographs of different types of nuclear abnormalities in erythrocytes of *Danio rerio* fish exposed to the etoposide solution (0.4 mg L^{-1}). **a** Micronucleus. **b** Binucleate. **c** Nuclear bud. **d** Cells with blebbed nucleus. **e** Lobed. **f** Notched. The arrows indicate the presence of micronucleated cells (magnification × 1000)

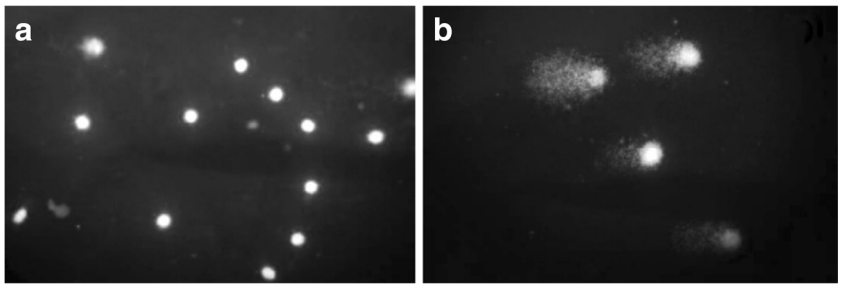

Fig. 10 Peripheral erythrocytes of *Danio rerio* with different cell damages. **a** Erythrocyte cells exposed to the solution after photocatalytic treatment, showing only cell types 0 and 1. **b** Exposure to etoposide solution (0.4 mg L^{-1}) showing damaged cell types 2, 3, and 4

the vertebral column and developmental abnormality of the yolk sac, and both these malformations are associated with the effects of the etoposide.

Because the results of the FET were not conclusive as to the toxicity caused by the initial solution of the drug and the solution treated by heterogeneous photocatalysis, we decided to carry out more thorough tests to measure the damage caused to the DNA in fish exposed to the initial solution as well as degradation products. Figure 9 depicts nuclear abnormalities and cells with micronuclei that were observed in fish erythrocytes exposed to the initial solution. Comparing the micronucleus frequencies between the groups exposed to treated etoposide residues with the control group, the photodegradation process can be seen to have eliminated the genotoxicity of the etoposide.

Figure 10a, b shows the results of comet assay in the fish peripheral erythrocytes exposed to the photocatalyzed (etoposide degraded solution) (Fig. 10a) and the etoposide original solution (Fig. 10b), clearly showing that degradation process significantly eliminated comet cells. In A there is no DNA damage. In B shows comet cells type 2, 3 and 4.

Table 2 shows the results of the micronucleus test and comet assay after exposure to etoposide, the photocatalytic degradation product, and the respective control group.

The micronucleus test is a cytogenetic test that evaluates chromosomal damage in a population exposed to mutagenic agents (Hayashi et al. 1992). Table 2 shows that micronucleus occurred only for the group exposed to the etoposide commercial solution, and no occurrence was identified for the control group or for the group exposed to the residues of the degraded etoposide.

Etoposide is well-known as a double-strand and single-strand DNA breaks inducer. This mechanism of action causes cell cycle delay promoting apoptosis and cell death. In an in vitro genotoxicity study, etoposide was exposed to zebrafish liver cells for comet and micronucleus assays. Induction of DNA breaks in the comet assay was more evident than in the micronuclei test (Gajski et al. 2016).

The comet assay is used to assess primary DNA damage in genotoxic compound identification studies (Tice et al. 2000). Low levels of damage were observed for both control group and the group exposed to degradation products. Statistical analysis between these two groups, however, did not show significant differences—ANOVA $P = 1.000$. The greatest damage was observed in the group exposed to the etoposide, demonstrating its genotoxic effects on fish. The results in Table 2 show that after the degradation treatment, both the mutagenic and genotoxic potential of the etoposide had been eliminated.

Table 2 Results of the micronucleus test and comet assay showing damages caused by initial etoposide solution (0.4 mg L^{-1}), the solution treated by heterogeneous photocatalysis and control

	Micronucleus ($n = 10$)	DNA damage index
Control	0	3.70 (± 0.95)
Etoposide	18	34.80 (± 9.46)*
Degradation product	0	4.12 (± 1.61)

*$p < 0.05$

Conclusion

The synthesis of $SrSnO_3$ by the combustion method proved to be efficient in obtaining the ceramic powder, which was confirmed by the characterization of the material. Most of the degradation processes, H_2O_2, UV, UV/H_2O_2, UV/$SrSnO_3$, showed low efficiency for etoposide mineralization. The UV/$SrSnO_3$/H_2O_2 process was the most efficient for degradation, reaching almost total mineralization, obtaining a rate of 97.98%, which was 1.35 times more efficient when compared with TiO_2, and the degradation rate was 3.02 times faster. The results of the zebrafish bioassays showed that the photocatalysis process eliminates the embryotoxic, genotoxic, and mutagenic effects of etoposide. Due to its increased use as an antineoplastic drug, residues of the drug have been found in aquatic environments, making the drug an emerging pollutant with mutagenic risks to aquatic biota. The development of a process to inactivate its mutagenic properties has become important to avoid further impact on aquatic organisms. Finally, we emphasize also that the photocatalysis developed in this study is an environmentally friendly process.

Acknowledgments The authors wish to thank the Brazilian funding agencies MCTI/CNPq (no. 483682 / 2013-6) and CAPES for their financial support, the Institute of Chemistry of the University of Brasília and

the Toxicologic Genetics Laboratory (G-TOX) of the Institute of Biological Sciences of the University of Brasília.

References

Alves MCF, Marinho RMM, Casali GP, Siu-Li M, Députier S, Guilloux-Viry M, Souza AG, Longo E, Weber IT, Santos IMG, Bouquet V (2013) Influence of the network modifier on the characteristics of $MSnO_3$ (M = Sr and Ca) thin films synthesized by chemical solution deposition. J Solid State Chem 199:34–41

Araceli G-A, Broséus R, Vincent S, Barbeau B, Prévost M, Sauvé S (2010) Oxidation kinetics of cyclophosphamide and methotrexate by ozone in drinking water. Chemosphere 79:1056–1063

Boczkaj G, Fernandes A (2017) Wastewater treatment by means of advanced oxidation processes at basic pH conditions: a review. Chem Eng J 320:608–633

Buerge IJ, Buser H-R, Poiger T, Muller MD (2006) Occurrence and fate of the cytostatic drugs cyclophosphamide and ifosfamide in wastewater and surface waters. Environ Sci Technol 40:7242–7250

Cabeza Y, Candela L, Ronen D, Teijon G (2012) Monitoring the occurrence of emerging contaminants in treated wastewater and groundwater between 2008 and 2010. The Baix Llobregat (Barcelona, Spain). J Hazard Mater 239:32–39

Cavalcante RP, Sandim LR, Bogo D, Barbosa AMJ, Osugi ME, Blanco M, Oliveira SC, Matos MFC, Junior AM, Ferreira VS (2013) Application of Fenton, photo-Fenton, solar photo-Fenton, and UV/H_2O_2 to degradation of the antineoplastic agent mitoxantrone and toxicological evalution. Environ Sci Pollut Res 20:2352–2361

Chen D, Ye J (2007) $SrSnO_3$ nanostructure: synthesis, characterization, and photocatalytic properties. Chem Mater 19:4585–4591

Crittenden JC, Hu S, Hand DW, Green SA (1999) A kinetic model for H_2O_2/UV process in a completely mixed batch reactor. Water Res 33:235–2328

Fenech M, Chang WP, Kirsch-Volders M, Holland N, Bonassi S, Zeiger E (2003) HUMN project: detailed description of the scoring criteria for the cytokinesis-block micronucleus assay using isolated human lymphocyte cultures. Mutat Res 534:65–75

Gajski G, Gerić M, Žegura B, Novak M, Nunić J, Bajrektarević D, Garaj-Vrhovac V, Filipič M (2016) Genotoxic potential of selected cytostatic drugs in human and zebrafish cells. Environ Sci Pollut Res 23:14739–14750

Hadjarab B, Bouguelia A, Trari M (2007) Synthesis, physical and photo electrochemical characterization of La-doped $SrSnO_3$. J Phys Chem Solids 68:1491–1499

Hayashi M, Kodama Y, Awogi T, Suzuki T, Asita AO, Sofuni T (1992) The micronucleus assay using peripheral blood reticulocytes from mitomycin C-and cyclophosphamide-treated rats. Mutat Res 278:209–213

Hernando M, Mezcua M, Fernández-Alba AR, Barceló D (2006) Environmental risk assessment of pharmaceutical residues in wastewater effluents, surface waters and sediments. Talanta 69:334–342

Hodjati S, Vaezzadeh K, Petit C, Pitchon V, Kiennemann A (2000) Absorption/desorption of NOx process on perovskites: performances to remove NOx from a lean exhaust gas. Appl Catal B Environ 26:5–16

Junploy P, Thongtem S, Thongtem T (2013) Photoabsorption and photocatalysis of $SrSnO_3$ produced by a cyclic microwave radiation. Superlattice Microst 57:1–10

Konstantinou IK, Albanis AT (2004) TiO_2-assisted photocatalytic degradation of azo dyes in aqueous solution: kinetic and mechanistic investigations: a review. Appl Catal B Environ 49:1–14

Kosmehl T, Hallare AV, Braunbeack T, Hollert H (2008) DNA damage induced by genotoxicants in zebrafish (Danio rerio) embryos after contact exposure to freeze-dried sediment and sediment extracts from Laguna Lake (The Philippines) as measured by the comet assay. Mutat Res 650:1–14

Lee CW, Kim DW, Cho IS, Park S, Shin SS, Seo SW, Hong KS (2012) Simple synthesis and characterization of $SrSnO_3$ nanoparticles with enhanced photocatalytic activitiy. Int J Hydrog Energy 37:10557–10563

Liu N, Zhang L, Xue Y, Lv J, Yu Q, Yuan X (2017) Nitrogen-doped carbon material as a catalyst for the degradation of direct red23 based on persulfate oxidation. Sep Purif Technol 184:213–219

Lobo TM, Lebullenger R, Bouquet V, Guilloux-Viy M, Santos IM, Weber IT (2015) $SrSnO_3$:N – nitridation and evaluation of photocatalytic activity. J Alloys Compd 649:1–15

Lucena GL, Souza JJN, Maia AS, Soledade LEB, Longo E, Souza AG, Santos IMG (2013) New methodology for faster synthesis of $SrSnO_3$ by the modified Pechini method. Cerâmica 59:249–253

Lutterbeck CA, Kern DI, Machado LE, Kummer K (2015) Evaluation of the toxic effects of four anti-cancer drugs in plant bioassays and its potency for screening in the context of waste water reuse for irrigation. Chemosphere 135:403–410

Ma Y, Li M, Wu M, Liu X (2015) Occurrences and regional distributions of 20 antibiotics in water bodies during groundwater recharge. Sci Total Environ 518:489–506

McEneff G, Schmidt W, Quinn B (2014) Pharmaceuticals in the aquatic environment: a short summary of current knowledge and the potential impacts on aquatic biota and humans. Environmental Protection Agency, Wexford, Ireland

National Cancer Institute (INCA) (2018) Brazil: Ministério da Saúde. INC; cl 996–2018 Availab from: http://www.inca.org.br. Accessed on February 02, 2018 (in Portuguese)

Nogueira RFP, Oliveira MC, Paterlini WC (2005) Simple and fast spectrophotometric determination of H_2O_2 in photo-Fenton reactions using metavanadate. Talanta 66:86–91

Nussbaumer S, Bonnabry P, Veuthey JL, Fleury-Souverain S (2011) Analysis of anticancer drugs: a review. Talanta 85:2265–2289

Ocampo-Pérez R, Sanchez-Polo M, Rivera-Utrillia J, Leyva-Ramos R (2010) Degradation of antineoplastic cytrabine inaqueous phase by advanced oxidation processes based on ultraviolet radiation. Chem Eng J 165:581–588

OECD (2013) Test No. 236: Fish embryo acute toxicity (FET) test. Oecd Publishing, Paris (OECD Guidelines for the Testing of Chemicals, Section 2)

Oller I, Malato S, Sánchez-Pérez J (2011) A combination of advanced oxidation processes and biological trataments for wastwater decontamination—a review. Sci Total Environ 409:4141–4166

Peña M, Fierro J (2001) Chemical structures and performance of perovskitas oxide. Chem Rev 101:1981–2017

Sales HS, Bouquet V, Députier S, Olivier S, Gouttefangeas F, Guilloux-Viry M, Santos IMG (2014) $Sr_{1-x}Ba_xSnO_3$ system applied in the photocatalytic discoloration of a an azo-dye. Solid State Sci 28:67–73

Solano A, da Silva G, Fialho S (2012) Development and validation of a high performance liquid chromatographic method for determination of etoposide in biodegradable polymeric implants. Quím Nova 35:1239–1243

Stahelin HF, Vin AW (1991) The chemical and biological route from podophyllotoxin glucoside to etoposide: Ninth Cain Memorial Award Lecture. Cancer Res 51:5–15

Tauc J (1966) The optical properties of solids. Academic Press, New York

Tice RR, Agurell E, Anderson D, Burlinson B, Hartmann A, Kobayashi H, Sasaki YF (2000) Single cell gel/comet assay: guidelines for in vitro and in vivo genetic toxicology testing. Environ Mol Mutagen 35:206–221

Verlicchi P, Galletti A, Petrovic M, Baceló D (2010) Hospital effluents as a source of emerging pollutants: An overview of micropollutants and sustainable treatment options. J Hydrol 389:416–428

Vogna D, Marotta R, Andreozzi R, Napolitano A, d'Ischia M (2004) Kinetic and chemical assessment of the UV/H_2O_2 treatment of antiepileptic drug carbamazepine. Chemosphere 54:497–505

Wang S, Zhou G, Zhang A, Yang Z (2007) Systematic investigations into $SrSnO_3$ nanocrystals (I) synthesis by using combustion and coprecipitation methods. J Alloys Compd 432:265–268

Wu JJ, Wu CC, Ma HW, Chang CC (2004) Treatment of landfill leachate by ozone-based advanced oxidation processes. Chemosphere 54: 997–1003

Yuan Y, Li XJZ, Yu T, Zou Z (2007) Large impact of strontium substitution on photocatalytic water splitting activity of $BaSnO_3$. Appl Phys Lett 91:094107

Yurdakal S, Loddo V, Augugliaro V, Berber H, Palmisano G, Palmisano L (2007) Photodegradation of pharmaceutical drugs in aqueous TiO_2: Mechanism and kinetics. Catal Today 129:9–15

Zeng MC, Huang D, Lai C, Xu P, Zhang C, Liu Y (2016) Hydroxyl radicals based advanced oxidation processes (AOPs) for remediation of soils contaminated with organic compounds: a review. Chem Eng J 284:582–598

Zhang W, Tang J, Ye J (2006) Photoluminescence and photocatalytic properties of $SrSnO_3$ perovskite. Chem Phys Lett 418:174–178